The 2019 World Congress on
Advances in Structural Engineering and Mechanics (ASEM19)
Jeju Island, Korea, September 17 - 21, 2019

Inversion analysis of three-dimensional initial geostress field of underground caverns of hydropower station

*Shun-Shun Li[1)] and Chao Su[2)]

[1), 2)] *College of Water Conservancy and Hydropower Engineering, Hohai University, Nanjing, 210098, China*
[1)] *shun-lee@qq.com*

ABSTRACT

The determination of initial in-situ stress field is very important for the design and construction of underground caverns of hydropower station. However, due to economic factors, it is impossible to measure on a large scale, and the initial in-situ stress field of the entire underground caverns construction area can only be obtained by inversion analysis under the condition of limited in-situ stress measurement points.This paper takes a hydropower station in southwest China as an example, and based on the measured data, The finite element multivariate regression method is used to inverse the three-dimensional initial in-situ stress field of underground caverns of hydropower stations. By comparing and verifying the inverted in-situ stress field with the measured data, it is found that the calculated stress value is in good agreement with the measured stress value. The results show that the inverted in-situ stress field is reasonable. At the same time, the distribution law of in-situ stress of underground caverns is analyzed, which has important reference value for the design and construction of underground caverns of hydropower station.

1. INTRODUCTION

In the stability analysis and support design of the surrounding rock of the underground cavern group of hydropower station, the initial in-situ stress field needs to be emphatically considered. The in-situ stress not only affects the stress redistribution of the surrounding rock after the excavation of the underground caverns, but also plays an important role in the deformation and stability of the surrounding rock. in-situ stress is one of the main causes of rock mass deformation and failure. In the design and construction of underground engineering, the initial in-situ stress field determines the supporting mode and parameters. The accuracy of the in situ stress field obtained by numerical simulation directly influences the final results, especially for excavations in high level tectonic stress areas (González de Vallejo and Hijazo, 2008). Thus, based on the measure- ment results and geological structure conditions, it is crucial to derive a reasonable stress field with wide applicability using a convenient and efficient back analysis approach coupled with an advanced numerical simulation method (Mckinnon, 2001; Saati and Mortazavi, 2011). Over the years, many scholars have proposed a variety of in-situ stress inversion methods. These methods include multiple linear

[1)] Graduate Student
[2)] Professor

regression analysis, artificial neural network methods (Li et al.,2012), and genetic algorithm optimization approaches (Grossberg, 1988; Kartam et al., 1997), which have been adopted extensively within stress boundary conditions and displacement boundary conditions in particular. (Guo *et al.,*1983) first put forward the principle of multiple regression to determine the initial in-situ stress field of rock mass.For the research and application of the neural network method,(Jiang et al., 2002) proposed the three-dimensional inverse analysis method of the initial in-situ stress field of artificial neural network in combination with the finite deformation theory, and inverted the initial in-situ stress field of practical engineering. For the research and application of genetic algorithm, (Fu et al.,2006) used genetic algorithm to invert the initial in-situ stress field of the whole dam area of Xi-Luo-Du hydropower station. For the underground powerhouse of the Three Gorges Project, the optimal displacement boundary conditions are used to fit the initial in-situ stress field (Guo et al.2008). Based on the measured in-situ stress data, an optimization function is established for any boundary displacement mode applied, and the displacement boundary mode is continuously adjusted. Finally, the optimal combination of boundary displacement modes and the initial in-situ stress field in the calculation range are obtained.The fitting effect of the inversion method of multivariate regression of the finite element mathematical model is good. Both gravity stress and tectonic stress are taken into account. The accuracy of the solution is high, which can ensure the reliability, rationality and uniqueness of the inversion results. Therefore, the method of multivariate regression is used to invert the three-dimensional initial geostress field of underground caverns.

2. Calculation principle

According to the multivariate regression method, the dependent variable is the in-situ stress regression calculation value $\hat{\sigma}_k$, and the independent variable is the stress calculation value $\hat{\sigma}_k$ of the corresponding measured point calculated by the finite element method, then the regression equation is:

$$\hat{\sigma}_k = \sum_{i=1}^{n} L_i \sigma_k^i$$

Among them, the sequence number of measuring points is *k*; the regression calculation value of *K* measuring points is $\hat{\sigma}_k$; the multiple regression coefficient is L_i; the single column matrix corresponding to the calculation value of six stress components is $\hat{\sigma}_k$ and σ_k^i; the working condition number is *n*.

Any stress state σ_k^i have the return of the corresponding calculated $\hat{\sigma}_k$. (Xiangbo et al., 2003)Define residuals of measured values $S_k = \sigma_k^* - \hat{\sigma}_k$ .If the number of measured points is *m*, the residual square sum of all measured values $\sum_{k=1}^{m}\sum_{j=1}^{6}\sigma_{jk}^*$ and regression calculated values $\sum_{k=1}^{m}\sum_{j=1}^{6}\hat{\sigma}_{jk}$ is used to represent the deviation degree between all measured values and regression equation:

$$S_r = \sum_{k=1}^{m}\sum_{j=1}^{6} S_{jk}^2 = \sum_{k=1}^{m}\sum_{j=1}^{6}\left(\sigma_{jk}^{*} - \sum_{i=1}^{n} L_i \sigma_{jk}^{i}\right)^2$$

In the formula, the measured value of *J* stress component at *k* point is σ_{jk}^{*}, and the calculated value of J stress component at k-point under *i* condition is σ_{jk}^{i}.

To minimize S_r, the equation must be satisfied (Qiangyong, et al., 2013) :

$$\begin{vmatrix} \sum_{k=1}^{m}\sum_{j=1}^{6}\left(\sigma_{jk}^{1}\right)^2 & \sum_{k=1}^{m}\sum_{j=1}^{6}\sigma_{jk}^{1}\sigma_{jk}^{2} & \cdots & \sum_{k=1}^{m}\sum_{j=1}^{6}\sigma_{jk}^{1}\sigma_{jk}^{n} \\ \sum_{k=1}^{m}\sum_{j=1}^{6}\sigma_{jk}^{1}\sigma_{jk}^{2} & \sum_{k=1}^{m}\sum_{j=1}^{6}\left(\sigma_{jk}^{2}\right)^2 & \cdots & \sum_{k=1}^{m}\sum_{j=1}^{6}\sigma_{jk}^{2}\sigma_{jk}^{n} \\ \vdots & \vdots & \ddots & \vdots \\ \sum_{k=1}^{m}\sum_{j=1}^{6}\sigma_{jk}^{1}\sigma_{jk}^{n} & \sum_{k=1}^{m}\sum_{j=1}^{6}\sigma_{jk}^{2}\sigma_{jk}^{n} & \cdots & \sum_{k=1}^{m}\sum_{j=1}^{6}\left(\sigma_{jk}^{n}\right)^2 \end{vmatrix} \begin{vmatrix} L_1 \\ L_2 \\ \vdots \\ L_n \end{vmatrix} = \begin{vmatrix} \sum_{k=1}^{m}\sum_{j=1}^{6}\sigma_{jk}^{*}\sigma_{jk}^{1} \\ \sum_{k=1}^{m}\sum_{j=1}^{6}\sigma_{jk}^{*}\sigma_{jk}^{2} \\ \vdots \\ \sum_{k=1}^{m}\sum_{j=1}^{6}\sigma_{jk}^{*}\sigma_{jk}^{n} \end{vmatrix}$$

By solving the equation, n regression coefficients $L = \left(L_1, L_2, \ldots, L_n\right)^T$ can be obtained, and the initial regression stress of P at any point in the calculation range is as follows:

$$\sigma_{jp} = \sum_{i=1}^{n} L_i \sigma_{jp}^{i}$$

For the above regression results, the complex correlation coefficient R is generally used to evaluate the regression effect.

$$R = \sqrt{1 - \frac{Q}{Q+U}} = \sqrt{\frac{U}{Q+U}}$$

The closer the complex correlation coefficient $0.0 \leq R \leq 1.0$ is to 1.0, (Chen et al., 2007) the better the regression effect will be.

3. Engineering example

3.1 project profile

A hydropower station is located in the upper reaches of Jinsha River of China. Its main buildings are intake, diversion tunnel, main powerhouse, bus tunnel, main transformer tunnel, tailrace tunnel, tailrace outlet, switch station, auxiliary powerhouse of central control building, outlet platform, traffic tunnel and exhaust tunnel. It is a large group of underground tunnels centered on main powerhouse. The water intake, tailrace outlet, switch station, auxiliary factory building of central control building and outlet platform are arranged on the ground. According to the coordination principle of geological structure and water conveyance line, the longitudinal axis direction of the main powerhouse is N37.68 degrees E.

The types of stratum rocks exposed on the surface are marble and amphibolite schist, chlorite amphibolite schist with mica quartz schist, marble strip and altered chlorite amphibolite schist. The surrounding rocks of underground cavern group are

mainly amphibolite schist, and the top arch and the right end wall are marble. According to the classification of cavern surrounding rocks, type II surrounding rocks account for 10%, type II surrounding rocks account for 55%, type III surrounding rocks account for 30%, and type IV surrounding rocks account for 5%. The main rock mechanics parameters are shown in Table 1.

Table 1 Main rock mechanics parameters used in calculation

Rock classification	density (g/cm3)	deformation modulus （GPa）	compressive strength （MPa）	Poisson's ratio	Shear strength parameters	
					Cohesive force （MPa）	Shear friction Coefficient
II_1	2.77	15	60	0.21	1.10	1.10
II_2	2.70	12	40	0.23	0.95	1.00
III	2.83	8	30	0.23	0.85	0.90
IV	2.70	3	15	0.26	0.30	0.70

3.2 Finite Element Model

According to the location of the main powerhouse and the size and layout of the first three caverns, the actual structure of underground caverns is simulated, including the main powerhouse, main transformer chamber, bus tunnel, main transformer transport tunnel, intake tunnel and tailrace tunnel. There are 623969 tetrahedral elements and 10 9116 nodes in the whole calculation model. The grid model of underground caverns is shown in Figure 7.

Scope of calculation: The upstream is bounded by the turning point of diversion tunnel, and the downstream boundary is 300 m from the downstream side wall of main transformer chamber; the axis direction of powerhouse is 600 m, the left side is bounded by river bed, and the right side is 200 m from the end wall of main powerhouse to the right side, of which four units are 120 m in total; the vertical boundary is bounded by the surface, and the lower boundary is 200 m from the bottom elevation of draft tube to the downstream. There are four faults which have great influence on the stability of surrounding rock: F6, F10, F14, F16. The relative position of faults and caverns is shown in Fig. 8.

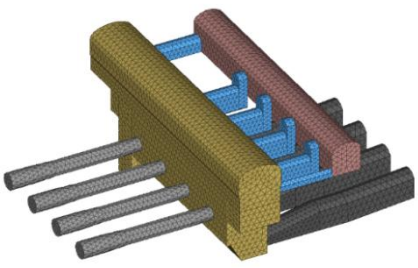

Fig. 1 Computational meshes for Underground caverns

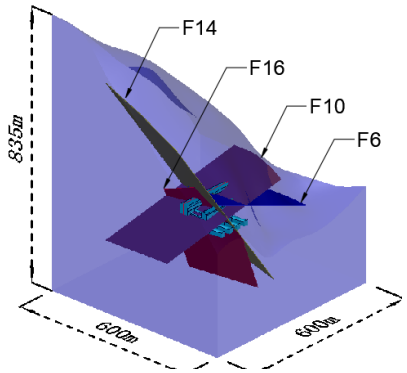

Fig. 2 Relative position of fault and caverns

3.3 Boundary Conditions

The factors affecting the initial in-situ stress field are very complex, including topography, lithology, geological structure, geotemperature and groundwater. (Jian-Guo et al., 2009) A large number of engineering practices show that gravity and geological tectonics are the main factors affecting the formation of in-situ stress field of rock mass, while the influence of geothermal and groundwater factors is relatively small and difficult to quantify, which can be neglected. Six factors, such as gravity of rock mass and geological tectonic movement, are selected as the main influencing factors in the regression analysis of initial in-situ stress. The specific boundary conditions applied in the regression calculation are as follows:

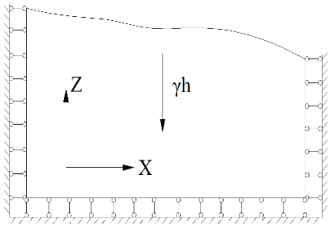

Fig.3 Self-weight stress model

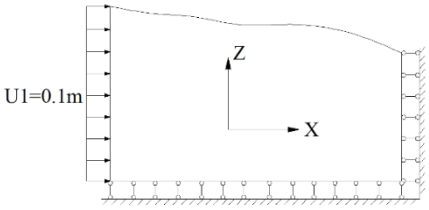

Fig.4 X horizontal extrusion stress model

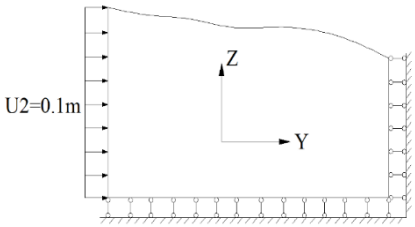

Fig. 5 Y horizontal extrusion stress model

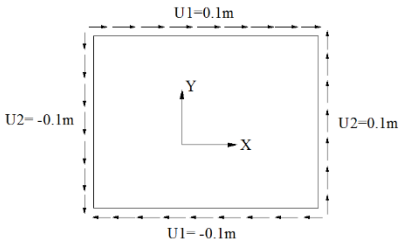

Fig. 6 XY shear stress model

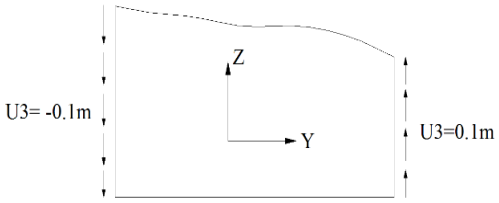

Fig.7 YZ shear stress model

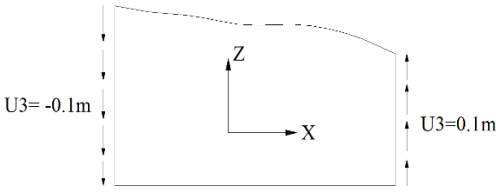

Fig.8 XZ shear stress n model

3.4 Measurement results of in-situ stress in engineering area

Three groups of in-situ stress tests have been done in the underground powerhouse area of the hydropower station. According to the measured data of PD11 (2557.6m elevation, 360m depth of the main tunnel), it can be seen that the lithology of the whole tunnel is chlorite amphibolite schist and amphibolite schis, and the occurrence of the rock layers is generally N20° ～50° W，SW∠35° ～50° , and the burial depth of the strong unloading level is about 10m and the weak unloading is not obvious; the burial depth of the weak weathering level is about 70m .

The in-situ stress test borehole ZK1 is located at the abutment of the dam site with an elevation of 3693m and a hole depth of 160.3m The borehole ZK2 is located at the riverbed of the dam site with an elevation of 3464m and a hole depth of 100.5m. In order to ensure the reliability of the data, nine representative boreholes are selected as

the basis for studying the in-situ stress field in the dam area. The measured stress data are shown in Table 2.

Table 2 Triaxial stress measurement results of rock mass in caverns area

number	σ_1			σ_2			σ_3		
	Value /MPa	Dip /(°)	Azimuth /(°)	Value /MPa	Dip /(°)	Azimuth /(°)	Value /MPa	Dip /(°)	Azimuth /(°)
ZK1-1	15.8	168.1	16.8	11.8	38.3	272.0	7.7	23.4	235.0
ZK1-2	14.4	26.7	170.8	9.8	31.4	278.7	4.7	46.5	48.7
ZK1-3	18.4	19.8	342.0	10.2	28.7	83.4	4.9	54.0	222.3
ZK2-1	15.3	17.8	354.1	8.8	-15.3	260.1	2.4	68.1	136.9
ZK2-2	16.8	3.6	158.6	9.8	-16.8	253.0	4.8	39.2	65.7
ZK2-3	16.2	22.4	149.1	9.1	50.5	29.1	1.9	30.6	253.2
ZK3-1	15.8	7.6	119.7	6.5	53.2	220.0	1.5	35.8	24.2
ZK3-2	12.6	8.1	293.8	7.5	44.4	195.8	2.1	44.5	31.8
ZK3-3	13.1	0.5	305.6	8.9	40.7	215.2	4.8	49.3	36.2

Note:
1) Geodetic coordinate system XYZ is defined as: X axis is north, Y axis is west, Z axis is vertical upward.
2) $\boldsymbol{\sigma}$ means the magnitude of the principal stress.

4. Analysis of in-situ stress inversion results

4.1 Stress Regression Coefficient

The regression coefficients $L_1 = 1.16$， $L_2 = 6.01$， $L_3 = -0.017$ $L_4 = -2.22$ $L_5 = 2.30$，$L_6 = 1.18$.(L_1 is the coefficient of self-weight stress. $L_2$is the coefficient of x-directional horizontal tectonic stress. L_3 is the coefficient of y-directional horizontal tectonic stress. $L_4$is the coefficient of xy-directional shear tectonic stress. $L_5$is the coefficient of yz-directional shear tectonic stress. $L_6$is the coefficient of zx-directional shear tectonic stress.) the regression equation of initial in-situ stress field is as follows:

$$\sigma_{\mathrm{e}} = 1.162\sigma_{\mathrm{s}} + 6.008\sigma_X - 0.017\sigma_Y - 2.22\sigma_{XY} + 2.30\sigma_{YZ} + 1.18\sigma_{ZX}$$

The multiple correlation coefficient R = 0.965 in regression analysis shows that the regression formula has good correlation.

4.2 Inversion Effect Evaluation

The comparison between the measured values of in-situ stress and the calculated values of regression is shown in Table 3. By comparing the measured and calculated values, the results show that the reasonable stress field distribution can be obtained by the regression analysis of the initial stress field through the three-dimensional numerical simulation of stress field and the fitting of the measured in-situ stress data. The results of regression analysis are in good agreement with the measured in-situ stress, which shows that the initial in-situ stress field calculated by multiple regression is reasonable and reliable.

Table 3 Comparisons between measured in-situ stress components and regression calculated values

number	category	σ_x (MPa)	σ_y (MPa)	σ_z (MPa)	τ_{xy} (MPa)	τ_{zx} (MPa)	τ_{yz} (MPa)
ZK1-1	measured	14.74	8.89	7.97	-1.89	-4.38	0.52
	Regression	14.77	8.67	7.75	-2.32	-3.97	0.98
ZK1-2	measured	12.59	8.19	8.01	-1.37	-3.43	1.78
	Regression	13.48	7.70	7.40	-2.21	-1.83	1.04
ZK1-3	measured	16.56	9.25	7.68	-1.99	3.34	-2.89
	Regression	17.00	9.34	8.85	-2.39	2.31	-1.06
ZK2-1	measured	12.17	10.44	3.86	-2.72	0.79	-3.83
	Regression	11.82	10.23	4.04	-1.93	-2.25	-1.70
ZK2-2	measured	16.06	7.53	7.86	-2.55	-2.50	-0.15
	Regression	16.51	6.97	7.65	-2.09	-0.85	1.91
ZK2-3	measured	14.38	4.54	8.24	-2.46	3.60	2.62
	Regression	14.81	5.12	8.73	-3.17	3.30	2.21
ZK3-1	measured	13.54	5.31	4.98	4.58	-1.62	2.23
	Regression	12.66	4.57	5.87	2.68	-2.08	1.11
ZK3-2	measured	12.32	7.91	6.53	-2.00	-1.85	-0.77
	Regression	11.92	8.07	5.92	-2.10	-1.79	-1.22
ZK3-3	measured	12.62	7.62	6.53	1.63	0.52	-1.94
	Regression	11.64	8.13	7.33	2.94	0.36.	-2.03

4.3 Law of stress distribution in in-situ stress field

(1) By comparing the nephogram of each stress component, it can be found that the value of in-situ stress increases with the increase of the thickness of the overburden.As shown in Figure 9,the value of each stress component near the fault zone varies obviously, and the change is mainly in the area near the lithological change interface; the shallow layer is greatly affected by the topographic change, and the contours are densely distributed near the surface and the valley, and the stress gradient varies greatly. It can be seen that the in-situ stress field in the engineering area is the stress field superimposed by tectonic stress and gravity stress. The initial in-situ stress field obtained by inversion fully reflects the influence of lithology, geological structure and topography.

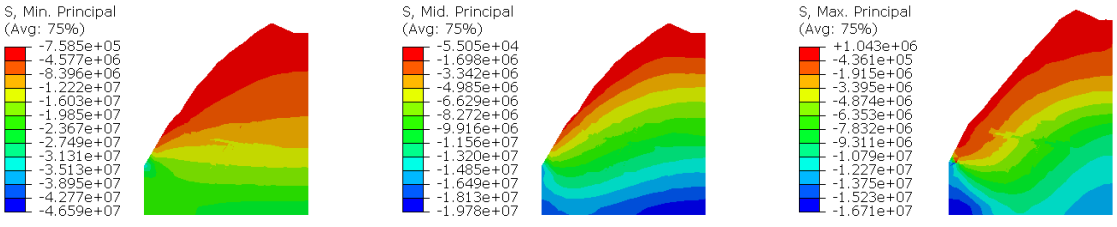

(a) maximum principal stress (b) Intermediate Principal Stress (c) Minimum principal stress

Fig.9 Distribution of Principal Stress of Mountain Body (Axis Direction of Main Powerhouse) (Unit: Pa)

(2) According to the distribution of in-situ stress field in 4 # unit-blocks, the distribution law of initial in-situ stress field is very similar, but due to the different thickness of overlying surrounding rock, the values of stress components are different. As shown in Figure 10,the stress_x along the axis of the factory building is 4.33-13.95 MPa, the stress_y along the axis of the vertical factory building is 7.26-12.05 MPa, and the vertical stress_z is 5.88-10.75 MPa. The stress components in the factory building area increase with the decrease of elevation. The magnitude and direction of the stress components near the fault area have undergone obvious mutations, which are mainly confined to a certain distance near the fault area and tend to be stable far away from the fault area.

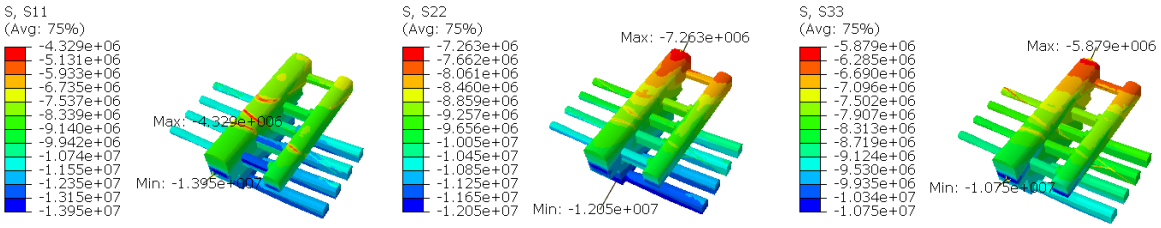

(a) Axis Direction (b) Downstream Direction (c) Vertical direction

Fig.10 Diagram of principal stress component distribution in caverns (Unit: Pa)

(3)As illustrated in Figure 11,the maximum principal stress of the main powerhouse is between 8.48 and 15.72 MPa, and the maximum compressive stress is at the bottom of the catchment well near the 1 # unit section of the main powerhouse; the minimum principal stress is between 1.22 and 10.01 MPa, and the minimum principal stress is at the junction of the main transporting tunnel and the fault F6. The rock mass in this area mainly consists of amphibolite schist, chlorite amphibolite schist, mica quartz schist, marble strip and altered chlorite amphibolite schist. The uniaxial saturated compressive strength is 40-60 MPa, which belongs to harder rock. The maximum principal stress of the main transformer chamber is between 9.31 and 14.37 MPa, the maximum compressive stress is at the bottom of the end wall of the main transformer chamber of pile No. CZ0+127.300, the minimum principal stress is between 1.24 and 9.74 MPa, and the minimum principal stress is near the arch where the main transformer tunnel intersects the fault F6.

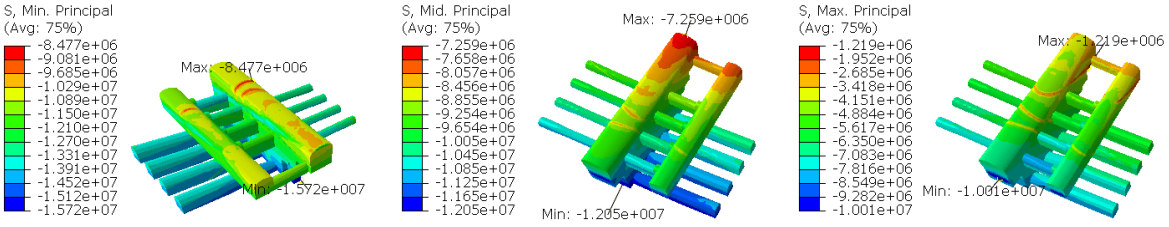

(a) maximum principal stress (b) Intermediate Principal Stress (c) Minimum principal stress

Fig.11 Schematic diagram of principal stress distribution in caverns model(Unit: Pa)

(4) The maximum principal stress and the minimum principal stress in the elevation plane in the generator layer is 11.05-14.49 MPa and 1.24-10.01 MPa respectively. The maximum principal stress in the elevation plane of bus layer is 10.75-14.49 MPa, and

the minimum principal stress is 3.06-8.35 MPa. The maximum principal stress in the elevation plane of the hydroturbine layer is 11.92-13.81 MPa, and the minimum principal stress is 3.72-7.78 MPa. It can be seen from the cross sections of hydroturbine layer, bus layer and generator layer in the workshop area that the initial in-situ stress at the same elevation varies due to the different thickness of the upper overburden layer. From the main workshop to the main transformer room, the covering thickness decreases gradually, and the values of principal stress and normal stress (absolute value) also decreases gradually.

5.Conclusion

Taking a hydropower station in southwest China as an example, considering the topographic and geomorphological characteristics of the valley and the geological structure conditions, the in-situ stress of the underground caverns of the hydropower station is inverted by the finite element multivariate regression method. According to the calculation results, it can be found that the in-situ stress increases with the increase of burial depth. The three-dimensional stresses of σ_x, σ_y and σ_z are orthogonal to each other, and the relationship between the values is $\sigma_x > \sigma_y > \sigma_z$. The maximum principal stress of the main powerhouse is between 8.48 and 15.72 MPa, and the maximum compressive stress is located at the bottom of the catchment well near the 1 # unit section of the main powerhouse. The maximum principal stress of the main transformer chamber is between 9.31MPa and 14.37MPa, and the maximum compressive stress is located at the bottom of the end wall of the main transformer chamber of pile number CZ0+127.300. Therefore, in the excavation and construction of underground powerhouse, strict attention should be paid to the position of maximum compressive stress. At the same time, the axis layout of underground powerhouse should be parallel to the maximum principal stress direction of the initial in-situ stress field and perpendicular to the minimum principal stress direction, which is beneficial to the stability of surrounding rock after excavation. Through regression analysis of underground powerhouse area, the in-situ stress value of key points obtained is close to the measured stress value, which shows that the inversion effect is better. The inversion reflects the distribution law of in-situ stress in the underground powerhouse area, and provides a reasonable three-dimensional initial stress field for the stability analysis of the excavation process of the powerhouse area caverns.

REFERENCES

Chen, X. T. , & Li, L. . (2007). Inverse analysis of initial field stress for underground cavities of a hydropower project. Rock & Soil Mechanics, 2007, 28 (5): 1523-1530.

Fu,C.H., Wang,W.M., Chen,S.H. “Back analysis study on initial geostress field of dam site for Xiluodu hydropower project. Chinese Journal of Rock Mechanics and Engineering,25 (11): 2305-2312.

González de Vallejo, L.I., Hijazo,T.(2008), “A new method of estimating the ratio between in situ rock stresses and tectonics based on empirical and probabilistic analyses”. Engineering Geology, 101(3-4):185-194.

Grossberg, S.,(1988). “Nonlinear neural networks: principles,mechanisms, and architectures”. Neural Networks, 1(1):17-61.

Guo ,H.Z., Ma, Q.C., Xue,X.C.,(1983). “Analysis method of initial stress field of rock mass. Chinese Journal of Geotechnical Engineering, 5 (3): 64-75.

Guo,M.W,Li,C.,Wang,S.L,et al., (2008). Study on inverse analysis of 3-D initial geostress field with optimized displacement boundaries. Rock and Soil Mechanics, 2008, 29(5): 1269-1274.

Jian-Guo, Z. , Qiang-Yong, Z. , Wen-Dong, Y. , & Xin, Z. . (2009). Regression analysis of initial geostress field in dam zone of dagangshan hydropower station. Rock & Soil Mechanics, 30(10), 3071-3078.

Kartam, N., Flood, I., Garrett, J.H.,(1997). “Artificial Neural Networks for Civil Engineers: Fundamentals and Applications”. American Society of Civil Engineers, New York, USA.

Li, Y.S., Yin, J.M., Chen, J.P., et al., (2012). “ Analysis of 3D in-situ stress field and query system’s development basedon visual BP neural network”. Procedia Earth and Plan-etary Science, 5:64-69.

Mckinnon,S.(2001),“Analysis of stress measurements using a numerical model methodology”. International Journal of Rock Mechanics and Mining Sciences,38(5):699-709.

Ming, J. Z. , Ya, X. W. , & Fu, S. J. . (2002). Ann-based 3-d back analysis of initial stress in rock masses. Journal of Hohai University, 30(3):52-56.

Qiangyong, Z. , Wen, X. , Xiuyong, Y. , & Xiaoping, H. . (2015). Back analysis of initial geostress field for underground powerhouse zone of shuangjiangkou hydropower station. China Civil Engineering Journal. 2015, 48 (8): 86-95.

Saati, V., Mortazavi, A. (2011) ,“Numerical modelling of in situ stress calculation using borehole slotter test”. Tunnelling and Underground Space Technology, 26(1):172-178.

Xiangbo, Q. , Shucai, L. , Shuchen, L. . (2003). 3d geostress regression analysis method and its application. Chinese Journal of Rock Mechanics & Engineering, 22(10), 1613-1617.